International Journal of
Information
and
Management
Sciences

International Journal of Information and Management Sciences
29 (2018), 345-363. DOI:10.6186/IJIMS.201812_29(4).0001

Rolling Bearing Fault Diagnosis Method Based on MOMEDA and IEWT

Zhi-Wu Shang, Geng Rui, Li Cheng, Liu Xia, Mao-Sheng Gao and Jin-Tian Yun

Tianjin Polytechnic University

Abstract

Aiming at the problem of early weak fault of non-stationary vibration signal in the background of complicated and heavy noises, a rolling bearing fault diagnosis technology based on multipoint optimal minimum entropy deconvolution adjusted (MOMEDA) and improved empirical wavelet transform (IEWT) is proposed. First, the acquired signal is analyzed by multipoint kurtosis (Mkurt) to obtain the approximate period of the signal and according to the obtained period, a reasonable period interval is determined. Using denoised method based on MOMEDA is to extract the periodic impulse of the original signal. Second, by using IEWT method, the denoised signal can be decomposed into number of intrinsic mode functions (IMFs). Finally, the IMFs are used the maximum kurtosis criterion for screening sensitive component, and then using Hilbert envelope spectrum analysis identifies the type of fault to achieve fault diagnosis. The experimental result shows that the proposed method can effectively improve the performance of fault diagnosis of rolling bearing.

Keywords: Rolling bearing, MOMEDA, EWT, non-stationary vibration signal, envelope spectrum.

1. Introduction

The rolling bearings are mechanical parts widely used in rotating machinery, its diagnosis will bring about equipment abnormal vibration and noise, and even unexpected accident proposed by Shi [10]. Therefore, the fault diagnosis of rolling bearing has been valued all the time. In the early detecting stage of heavy noise and weak fault of the bearings, Ma et al. [5] combine with the principle of Morlet wavelet transform and propose a method of determining the optimal scale parameters from the scale-related power distribution, which provides an effective way to extract the feature of early weak fault signals in the bearing. Ren et al. [8] propose an early bearing fault diagnosis based on dual-tree complex wavelet transform adaptive Teager energy spectrum and the effectiveness of the proposed method is verified by simulation and experimental data. These methods all contribute to the diagnosis and research of early bearing fault.

Wang et al. [12] discussed that the denoised methods which are commonly used in fault diagnosis include band-pass filter, morphological filtering, wavelet denoising and empirical mode decomposition (EMD). Among them, the wavelet denoising is widely used in the field of signal processing due to its multi-resolution characteristics. Hu et al. [3], Wang et al. [15] and Ma et al. [6] use wavelet denoising for the feature extraction of early weak faults in rolling bearings, but the wavelet basis and the selection of decomposition scale are not adaptive and difficultly apply to complicated signals. The EMD is a completely adaptive method proposed by Li et al. [4]. Aiming at the end effects of EMD, Shi et al. [9] proposed an improved method of combining waveform feature matching extension with cosine window function, which is better to restrain the end effects. Zhang et al. [16] firstly decomposed the weak fault signals into intrinsic mode functions (IMFs) by using EMD, and then used the sliding kurtosis algorithm to process the IMFs and extract the fault feature frequency, and ultimately achieve satisfactory results. Although many improvements have been made, there exists still some problems such as modal mixing, under-envelope, over-envelope and end effects in the EMD. Therefore, Gilles [2] put forward a new adaptive signal processing method called empirical wavelet transform (EWT) based on the framework of the wavelet transform and EMD. The advantages of the method not only lie in the ability of constructing suitable orthogonal wavelet filter banks, segmenting the Fourier spectrum of the signal and extracting the amplitude modulated-frequency modulated (AM-FM) components with compact support, but also there exists no mode mixing, and the negative frequency caused by Hilbert transform, etc. However, Zheng et al. [18], Shi et al. [11] and Wang et al. [13] all argued that the spectrum segmentation which is required by EWT strongly relies on local maxima of its amplitudes and spends a lot of calculation time. Hence, an improved empirical wavelet transform (IEWT) is proposed. The new segmentation approach performs envelope analysis on the Fourier spectrum of the signal. Then the frequency which corresponds to the local minima point of the envelope is marked, that is the locations of the spectrum segmentation boundaries.

However, the weak fault signals are often overwhelmed by heavy noise and other strong vibration components, which leads to less obvious fault feature in the IMFs. Therefore, it is particularly important how to effectively reduce the interference of heavy noise and highlight faulty feature. McDonald and Zhao [7] proposed a denoised method based on MOMEDA. This method is suitable for periodic fault feature extraction. The approximate period of fault is determined by multipoint kurtosis (Mkurt), and then setting a reasonable period interval is to effectively extract the periodic impulse overwhelmed by heavy noise and other strong vibration components, and thus, this method reduces noise and improves the original signal kurtosis, this method was also discussed by Wang et al. [14].

Based on above discussions, this paper proposes a bearing fault diagnosis method based on MOMEDA and IEWT. The experimental results show that the noise can be well suppressed, and the faulty feature can be effectively extracted by the proposed method.

The remainder of this paper is organized as follow. In Section 2, the algorithms of the MOMEDA and EWT method are briefly reviewed. Then, the IEWT method is

proposed for well segmenting the Fourier spectrum of the signal. Section 3 describes the algorithm flow of the proposed method in detail. Section 4 performs the simulation study based on two signals, and the IEWT method is compared with the EMD and EWT method. In Section 5, the proposed method is applied for fault diagnosis of the inner race of the bearing. Section 6 summarizes the conclusions in this paper.

2. Theoretical Study

2.1. Multipoint optimal minimum entropy deconvolution adjusted technique

Cabrelli and Carlos [1] defined a new criterion for the varimax norm: the D-norm, which is obtained through the modification of the kurtosis norm when multiple data inputs. The D-norm deconvolution problem is non-iterative solution for computing the filter coefficients. Therefore, McDonald proposed a deconvolution algorithm called MOMEDA based on multi D-norm (MDN) for the target recognition of multiple impulses. The algorithm is mainly applied to the fault feature extraction of periodic impulses.

When the bearing occurs the fault, given an acquired discrete signal:

$$y(n) = h(n) * x(n) + e(n) \tag{2.1}$$

where $e(n)$ is the white noise, $x(n)$ is an impulse train modeling a fault, $h(n)$ is the transfer function and $y(n)$ is the acquired vibration signal.

The MOMEDA algorithm proposed by McDonald is to find a FIR filter $w(l)$ and to make the impulse train $x(n)$ restore the input signal $y(n)$ as much as possible. The core of the algorithm is to recognize the goal impulses at known locations. Hence, we introduce this maximization problem as the MOMEDA:

$$MDN(\boldsymbol{y}, \boldsymbol{t}) = \frac{1}{\|\boldsymbol{t}\|} \frac{\boldsymbol{t}^T \boldsymbol{y}}{\|\boldsymbol{y}\|} \tag{2.2}$$

$$\max\ MDN(\boldsymbol{y}, \boldsymbol{t}) = \max_f \frac{\boldsymbol{t}^T \boldsymbol{y}}{\|\boldsymbol{y}\|} \tag{2.3}$$

where the above $\boldsymbol{t}$ is a constant vector that determines location and weighting of the goal impulses.

Through taking the derivative of filter coefficients ($\boldsymbol{f} = f_1, f_2, \ldots, f_L$) to get the extrema of Eq. (2.3):

$$\frac{d}{d\boldsymbol{f}}\Big(\frac{\boldsymbol{t}^T \boldsymbol{y}}{\|\boldsymbol{y}\|}\Big) = \frac{d}{d\boldsymbol{f}} \frac{t_1 y_1}{\|\boldsymbol{y}\|} + \frac{d}{d\boldsymbol{f}} \frac{t_2 y_2}{\|\boldsymbol{y}\|} + \cdots + \frac{d}{d\boldsymbol{f}} \frac{t_{N-L} y_{N-L}}{\|\boldsymbol{y}\|} \tag{2.4}$$

Since $\dfrac{d}{d\boldsymbol{f}} \dfrac{t_k y_k}{\|\boldsymbol{y}\|} = \|\boldsymbol{y}\|^{-1} t_k \boldsymbol{M}_k - \|\boldsymbol{y}\|^{-3} t_k y_k X_0 \boldsymbol{y}$ and $\boldsymbol{M}_k = \begin{bmatrix} x_{k+L-1} \\ x_{k+L-2} \\ \vdots \\ x_k \end{bmatrix}$, Eq. (2.4) can be written:

$$\frac{d}{d\boldsymbol{f}}\Big(\frac{\boldsymbol{t}^T \boldsymbol{y}}{\|\boldsymbol{y}\|}\Big) = \|\boldsymbol{y}\|^{-1}(t_1 \boldsymbol{M}_1 + t_2 \boldsymbol{M}_2 + \cdots + t_{N-L} \boldsymbol{M}_{N-L}) - \|\boldsymbol{y}\|^{-3} \boldsymbol{t}^T \boldsymbol{y} X_0 \boldsymbol{y}. \tag{2.5}$$

With the simplification,

$$t_1\boldsymbol{M}_1 + t_2\boldsymbol{M}_2 + \cdots + t_{N-L}\boldsymbol{M}_{N-L} = X_0\boldsymbol{t}.$$

And solving the extrema by equaling to $\mathbf{0}$, Eq. (2.5) becomes:

$$\|\boldsymbol{y}\|^{-1}X_0\boldsymbol{t} - \|\boldsymbol{y}\|^{-3}\boldsymbol{t}^T\boldsymbol{y}X_0\boldsymbol{y} = \mathbf{0}.$$

That is $\dfrac{\boldsymbol{t}^T\boldsymbol{y}}{\|\boldsymbol{y}\|^2}\boldsymbol{X}_0\boldsymbol{y} = \boldsymbol{X}_0 t.$

Since $\boldsymbol{y} = X_0^T\boldsymbol{f}$ and assuming $(\boldsymbol{X}_0\boldsymbol{X}_0^T)^{-1}$ exists:

$$\frac{\boldsymbol{t}^T\boldsymbol{y}}{\|\boldsymbol{y}\|^2}\boldsymbol{f} = (X_0X_0^T)^{-1}X_0\boldsymbol{t}. \tag{2.6}$$

Since multiples of $\boldsymbol{f}$ are also the solutions to Eq. (2.6), multiples of $\boldsymbol{f} = (X_0X_0^T)^{-1}X_0\boldsymbol{t}$ are solutions to the MOMEDA problem.

The MOMEDA filter and output solutions can be simply summarized as:

$$\boldsymbol{f} = (X_0X_0^T)^{-1}X_0\boldsymbol{t} \tag{2.7}$$

$$X_0 = \begin{bmatrix} x_L & x_L & x_{L+2} & \cdots & x_N \\ x_{L-1} & x_L & x_{L+1} & \cdots & x_{N-1} \\ x_{L-2} & x_L & x_L & \cdots & x_{N-2} \\ \vdots & \vdots & \vdots & \ddots & \vdots \\ x_1 & x_2 & x_3 & \cdots & x_{N-L+1} \end{bmatrix}. \tag{2.8}$$

$$\boldsymbol{y} = X_0^T\boldsymbol{f}. \tag{2.9}$$

$\boldsymbol{t}$ has the same length as the output $N - L + 1$, and represents the location and weighting of the deconvolution impulses in the output. The MOMEDA method obtains the non-iterative optimal solution, which provides the basis for the periodic fault diagnosis of rotating machinery. The MOMEDA method can be calculated for M contiguous target vectors $\boldsymbol{t}_1, \boldsymbol{t}_2, \ldots, \boldsymbol{t}_M$. In this case, Eq. (2.7) and Eq. (2.9) become Eq. (2.10) and Eq. (2.11).

$$F = [\boldsymbol{f}_1\boldsymbol{f}_2\cdots\boldsymbol{f}_M] = (X_0X_0^T)^{-1}X_0[\boldsymbol{t}_1\boldsymbol{t}_2\cdots\boldsymbol{t}_M] \tag{2.10}$$

$$Y = [\boldsymbol{y}_1\boldsymbol{y}_2\cdots\boldsymbol{y}_M] = \boldsymbol{X}_0^T F. \tag{2.11}$$

Due to MOMEDA denoised method, the location of deconvolution impulse is uniquely determined. In the whole sampling interval, there only exists an impulse each period. In the background of heavy noise, in order to further extract the impulses, the location of deconvolution impulse can be accurately controlled by setting the interval of the denoised period. Therefore, the multipoint kurtosis (Mkurt) is introduced as the measure of faulty feature extraction, the unnormalized Mkurt is defined as follow:

$$\mathrm{Mkurt}(\boldsymbol{y}, \boldsymbol{t}) = k\frac{\sum_{n=1}^{N-L}(t_ny_n)^4}{\Big(\sum_{n=1}^{N-L}y_n^2\Big)^2}. \tag{2.12}$$

When output $\boldsymbol{y}$ is equal to target vector $\boldsymbol{t}$, the Mkurt gets normalized as:

$$k\frac{\sum\limits_{n=1}^{N-L}(t_n^2)^4}{\Big(\sum\limits_{n=1}^{N-L}t_n^2\Big)^2}=1. \tag{2.13}$$

Get the normalization factor:

$$k=\frac{\Big(\sum\limits_{n=1}^{N-L}t_n^2\Big)^2}{\sum\limits_{n=1}^{N-L}t_n^8}. \tag{2.14}$$

Finally, the normalized Mkurt is described as follows:

$$\text{Mkurt}=\frac{\Big(\sum\limits_{n=1}^{N-L}t_n^2\Big)^2}{\sum\limits_{n=1}^{N-L}t_n^8}\frac{\sum\limits_{n=1}^{N-L}(t_ny_n)^4}{\Big(\sum\limits_{n=1}^{N-L}y_n^2\Big)^2}. \tag{2.15}$$

This definition is based on kurtosis, but its target vector is expanded into multiple impulses at the controlled location and further normalized.

2.2. Empirical wavelet transform

The purpose of EMD is to decompose the signal $f(t)$ into sum of $N+1$ IMFs $f_k(t)$ such that:

$$f(t)=\sum_{k=0}^{N}f_k(t). \tag{2.16}$$

An IMF is defined as AM-FM function which is described as follow:

$$f_k(t)=F_k(t)\cos(\Phi_k(t)),\quad F_k(t)>0,\quad \Phi_k'(t)>0. \tag{2.17}$$

The change rate of $F_k(t)$ and $\phi_k(t)$ is slower than ϕ_k. In the EMD method, what is the most interest is how to adaptively select the AM-FM component from the original signal $f_k(t)$. The classic EMD method results in the mode mixing and end effect due to the unreasonable stop criteria, upper and lower envelope problems. Moreover, the screening process of the EMD method also lacks of mathematical theory. To overcome this problem, Gilles combined the wavelet transform with the adaptive EMD, and proposed the EWT method. This method is based on the theoretical framework of wavelet analysis and selects a set of wavelet filter banks to adaptively extract the different AM-FM components according to the Fourier spectrum of the signal. To select a suitable wavelet filter bank, the Fourier spectrum needs to be adaptively segmented. Assume that the Fourier support $[0,\pi]$ is segmented into N continuous segments. We denote ω_n to be the boundary limits

between each segments ($\omega_n = 0$, $\omega_N = \pi$), the ω_n is chosen as the midpoint between two adjacent maxima for the signal Fourier spectrum, As shown in Figure 1, each segments can be expressed as follow:

$$\begin{cases} \Lambda_n = [\omega_{n-1}, \omega_n], \ n = 1, 2, \ldots, N \\ \bigcup_{n=1}^{N} \Lambda = [0, \pi] \end{cases} \tag{2.18}$$

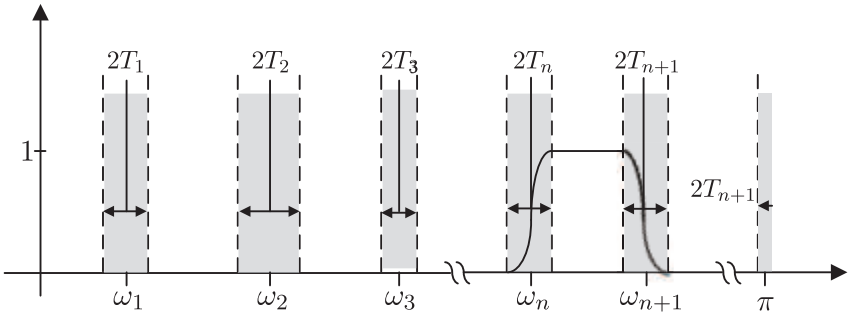

Figure 1: The Spectrum Segmentation.

Centered on each and the width T_n is equal to $2\tau_n$, a transition phase is defined, as shown in the shaded area in Figure 1.

After determining the segmentation interval Λ_n, the empirical wavelets are defined as the bandpass filters on each Λ_n. Gilles constructed the empirical wavelets based on the construction method of Meyer wavelet, the empirical wavelets function $\hat{\psi}_n(\omega)$ and empirical scaling function $\hat{\varphi}_n(\omega)$ are defined as follows:

$$\hat{\psi}_n(\omega) = \begin{cases} 1, & (1+\gamma)\omega_n \le |\omega| \le (1-\gamma)\omega_{n+1} \\ \cos\left[\frac{\pi}{2}\beta\Big(\frac{1}{2\gamma\omega_{n+1}}(|\omega| - (1-\gamma)\omega_{n+1})\Big)\right], & (1-\gamma)\omega_{n+1} \le |\omega| \le (1+\gamma)\omega_{n+1} \\ \sin\left[\frac{\pi}{2}\beta\Big(\frac{1}{2\gamma\omega_n}(|\omega| - (1-\gamma)\omega_n)\Big)\right], & (1-\gamma)\omega_n \le |\omega| \le (1+\gamma)\omega_n \\ 0, & \text{otherwise} \end{cases} \tag{2.19}$$

$$\hat{\varphi}_n(\omega) = \begin{cases} 1, & |\omega| \le (1-\gamma)\omega_n \\ \cos\left[\frac{\pi}{2}\beta\Big(\frac{1}{2\gamma\omega_n}(|\omega| - (1-\gamma)\omega_n)\Big)\right], & (1-\gamma)\omega_n \le |\omega| \le (1+\gamma)\omega_n \\ 0, & \text{otherwise} \end{cases} \tag{2.20}$$

Where:

$$\beta(x) = x^4(35 - 84x + 70x^2 - 20x^3) \tag{2.21}$$

$$\tau_n = \gamma\omega_n \quad \text{and} \quad \gamma < \min_n\Big(\frac{\omega_{n+1} - \omega_n}{\omega_{n+1} + \omega_n}\Big). \tag{2.22}$$

Reference to the construction method of classic wavelet transform, the detail coefficients are defined as followed:

$$W_f^{\varepsilon}(n,t) = \langle f, \psi_n \rangle = \int f(\tau)\overline{\psi_n(\tau - t)}d\tau = \Big(\hat{f}(\omega)\overline{\hat{\psi}_n(\omega)}\Big)^{\vee} \tag{2.23}$$

$$W_f^{\varepsilon}(0,t) = \langle f, \phi_1 \rangle = \int f(\tau)\overline{\phi_1(\tau - t)}d\tau = \left(\hat{f}(\omega)\overline{\hat{\phi}_1(\omega)}\right)^{\vee} \tag{2.24}$$

where $\hat{\psi}_n(\omega)$ and $\hat{\phi}_1(\omega)$ represent the Fourier transform function of $\psi_n(t)$ and $\phi_1(t)$, respectively. $\overline{\psi_n(\omega)}$ and $\overline{\phi_1(t)}$ represent complex conjugate function of $\psi_n(t)$ and $\phi_1(t)$, respectively. $\langle\ ,\ \rangle$ is defined as the inner product.

As a result, the reconstruction of the signal $f(t)$ is obtained as follow:

$$\begin{aligned} f(t) &= W_f^{\varepsilon}(0,t) * \phi_1(t) + \sum_{n=1}^{N} W_f^{\varepsilon}(n,t) * \psi_n(t) \\ &= \left(\hat{W}_f^{\varepsilon}(0,\omega)\hat{\phi}_1(\omega) + \sum_{n=1}^{N} \hat{W}_f^{\varepsilon}(n,\omega)\hat{\psi}_n(\omega)\right)^{\vee}. \end{aligned} \tag{2.25}$$

The signal $f(t)$ is decomposed into AF-FM component $f_j(t)$ $(j = 0, k;\ k = 1, 2, 3, \ldots)$ by the EWT method which can be written in the form:

$$f_{j=0}(t) = W_f^{\varepsilon}(0,t) * \phi_1(t) \tag{2.26}$$

$$f_{j=k}(t) = W_f^{\varepsilon}(k,t) * \phi_k(t) \tag{2.27}$$

where $*$ is convolution calculation operator.

2.3. Improved Empirical Wavelet Transform

Based on EWT theoretical framework and upper envelope analysis, the IEWT algorithm is proposed, which can adaptively segment the Fourier spectrum of the signal. Firstly, the new segmentation approach performs upper envelope analysis on the spectrum of the signal. Then the frequency which corresponds to the local minima point of the envelope is marked, that is the locations of the spectrum segmentation boundaries. Finally, the Meyer wavelet filtering is performed on the segmentation region. Such a spectrum segmentation method does not require extensive calculation time. For example, assuming the vibration signal $x(t)$, Its IEWT method can be implemented through the following steps:

(1) Construct the Fourier transform of $x(t)$, such that

$$F(s) = |fft(x)| \tag{2.28}$$

(2) Know the Fourier function $F(s)$ from step (1), in the interval $[0, f]$, look for $N + 1$ nodes, $0 = f_0 < f_1 < \cdots < f_n = f$ and $\underset{0 \le i \le n}{fi} \notin (f_p - mpd, f_p + mpd)$, where f is the sampling rate, f_i is the node frequency, f_p is the local peak frequency, mpd is the minimum peak distance which ignores the smaller meaningless peaks that may be generated nearly local larger peaks.

(3) Via these nodes, using the spline interpolation method is to generate the upper envelope curve of the Fourier spectrum.

(4) Find the minima point of the envelope curve as the locations of the spectrum segmentation boundaries, that is $\omega_i = [\omega_0, \omega_1, \ldots, \omega_N]$.

(5) According to the segmented frequency band, applying the Meyer wavelet construction method in EWT theory is to construct the empirical wavelet which realizes the mode decomposition.

This method does not need to set the number of segmentations of the Fourier spectrum in advance and saves a lot of calculation time, and was verified by Zhu and Feng [19]. Only through the minima points of the envelope curve, can it effectively segment the spectrum.

3. Diagnostic Algorithm Design

Based on the above analysis, in order to enhance the fault feature extraction, an early fault diagnosis method of rolling bearing based on MOMEDA and IEWT is proposed. The algorithm is designed as follows:

(1) Calculate the Mkurt of the fault signal and determine the approximate period of the fault, and then set a reasonable fault period interval.

(2) The MOMEDA denoised method is used to extract the impulse components of the fault signal for enhancing the fault feature.

(3) The IEWT method is used to realize the adaptive mode decomposition of the vibration signal for obtaining significant multiple component signals.

(4) Perform kurtosis analysis for the decomposed multiple component signal and select the largest component of kurtosis.

(5) The screened sensitive component is analyzed by Hilbert envelope spectrum and bearing fault feature is identified by the acquired spectrum.

4. Simulation Study

To verify the feasibility and effectiveness of the proposed method, the simulation signal $x_1(t)$ and $x_2(t)$ are constructed, and compared with the EMD and EWT methods, respectively.

4.1. Simulation signal $x_1(t)$

The simulation signal $x_1(t)$ is composed of three constitutes, including the sinusoidal signal $x_{11}(t)$, the AM-FM signal $x_{12}(t)$ and $x_{13}(t)$. The signal time-domain waveforms are shown in Figure 2, the sampling frequency is 2000Hz, the sampling time is 1s, such that

$$\begin{cases} x_{11}(t) = \sin(50\pi t) \\ x_{12}(t) = (1 + \sin(10\pi t)) \sin(200\pi t + \cos(20\pi t)) \\ x_{13}(t) = (1.5 + \sin(10\pi t)) \sin(400\pi t + \cos(20\pi t)) \\ x_1(t) = x_{11}(t) + x_{12}(t) + x_{13}(t). \end{cases} \tag{4.1}$$

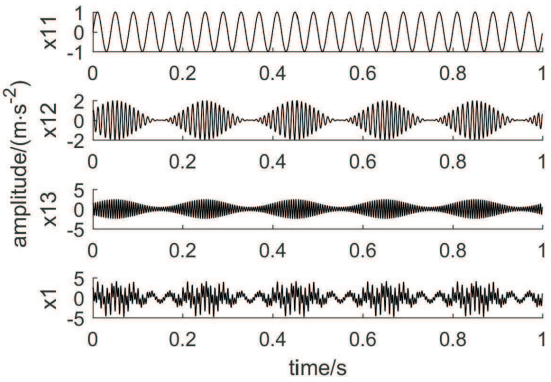

Figure 2: The Time-domain waveforms of the simulation signal.

For the comparison, firstly, the EWT method is used to segment the Fourier spectrum, the number of spectrum segmentation is 4, as shown in Figure 3(a). According to the peaks of the spectrum, the EWT respectively decomposes the signal $x_{11}(t)$ and $x_{12}(t)$ into single component, but the signal $x_{13}(t)$ is decomposed into two components due to fitting errors, which resulting in appearing the false components. The decomposition result is given in Figure 3(b), in which the result has some differences from the true components.

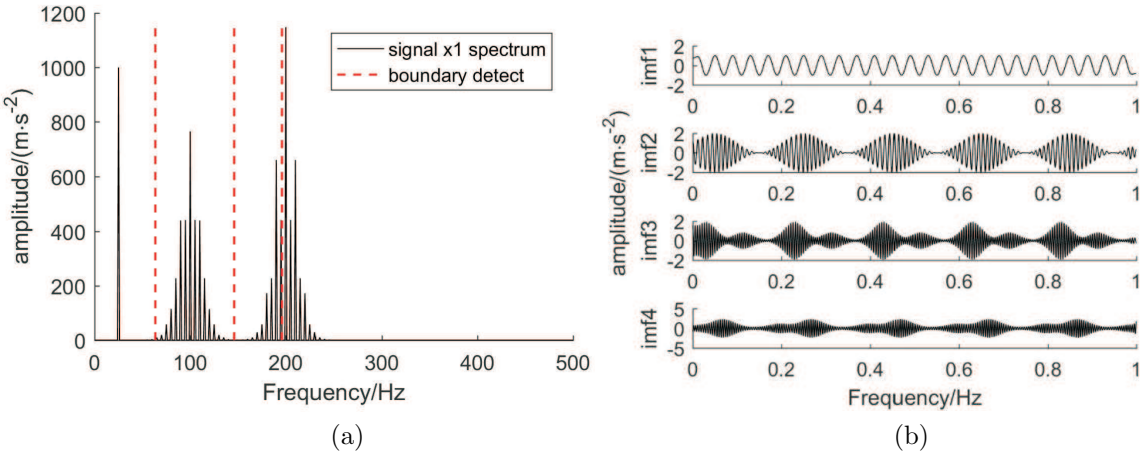

(a) (b)

Figure 3: (a) The EWT spectrum segmentation; (b) The EWT decomposition result.

Then, the signal $x_1(t)$ can be completely decomposed into the three components by using IEWT adaptive spectrum segmentation method as shown in Figure 4(a), it can be clearly seen from the figure that the Fourier spectrum is adaptively segmented into three parts by IEWT method according to the upper envelope area, and determined two spectrum segmentation boundaries. The frequency center the decomposition result is 25Hz, 100Hz and 200Hz, corresponding to the true components $x_{11}(t)$, $x_{12}(t)$ and $x_{13}(t)$, respectively. The Figure 4(b) shows the decomposition result of the IEWT method.

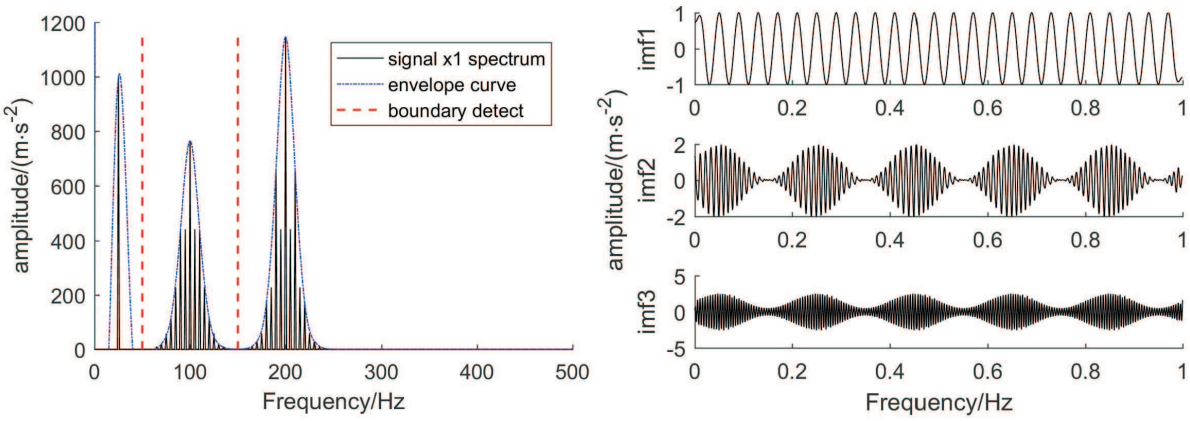

(a) (b)

Figure 4: (a) The IEWT spectrum segmentation; (b) The IEWT decomposition result.

To be compared with IEWT method, Figure 5(a) shows the multiple component obtained by the EMD method. The EMD obtains the twelve IMFs, due to space limitations, this article only lists the first six mode components. It can be found that the later IMFs are false components. Moreover, the Fourier transform is employed for IMF1, and the result of frequency-domain is shown in Figure 5(b). We can see that from Figure 5(b) there exists serious mode mixing problems, which is not favorable to fault feature extraction.

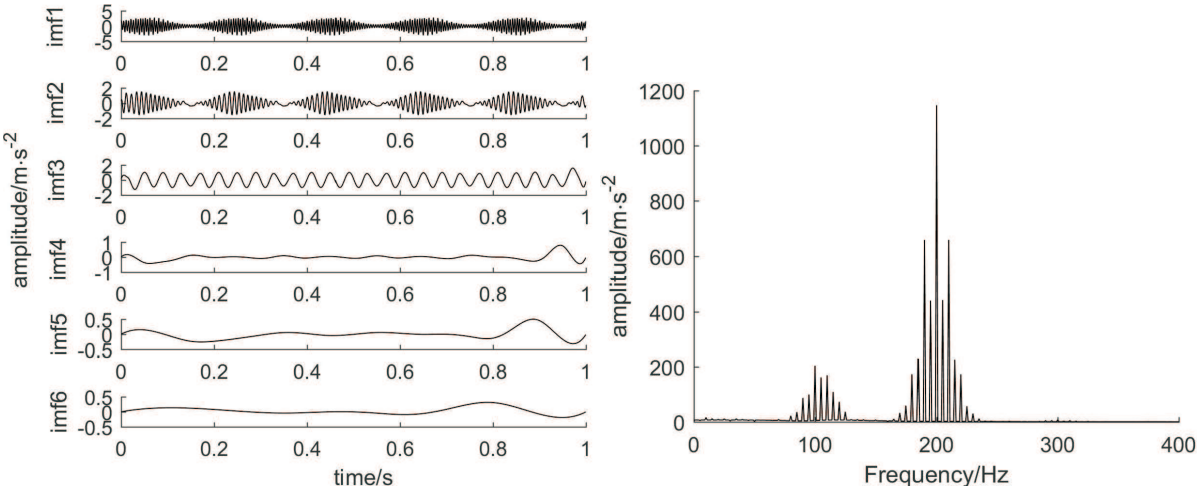

(a) (b)

Figure 5: (a) The EMD decomposition result; (b) The frequency-domain result of IMF1.

In summary, The IEWT method can adaptively decompose the signals, eliminate mode mixing and retain sideband information, which is suitable for fault diagnosis of rolling bearings.

4.2. Simulation signal

The simulation signal $x_2(t)$ uses Randall's rolling bearing model to simulate the pitting fault in the bearing inner race, this model was used by Zhao and Li [17]. To facilitate the analysis, in the establishment of the bearing AF-FM vibration signal model, only considering the bearing fault feature frequency, so given the simplified model of the bearing vibration signal can be written as:

$$\begin{cases} x_2(t) = \sum_{i=1}^{M} p(t - iT) + n(t) \\ p(t) = e^{-Ct}\cos(2\pi f t) \end{cases} \tag{4.2}$$

where M is the number of the periodic impulses; T is the period of the impulses; $p(t)$ is the oscillating waveform generated by a single impulse; the resonance frequency f of the bearing is 4000Hz; the attenuation coefficient C is equal to the constant of 800, the determined value relates to the bearing type; the sampling frequency f_s is 20KHz; The fault frequency of the bearing inner race $f_i = f_s/T = 50$Hz; $n(t)$ is an additive background noise, the signal-to-noise ratio(SNR) is -15dB.

According to the above model, the simulation signal of the bearing inner race fault is generated, Figure 6(a) shows the waveform of the fault impulse and Figure 6(b) shows the simulation signal of additive noise. Compared Figure 6(a) and Figure 6(b), it can be clearly seen that when the heavy noise appears, the information of the impulse is almost completely overwhelmed. The Hilbert envelope spectrum analysis is applied for the simulation signal and the results is shown in Figure 7. It can be seen that there exists almost obvious amplitude component in the envelope spectrum, so the fault features of the bearing inner race cannot be effectively extracted.

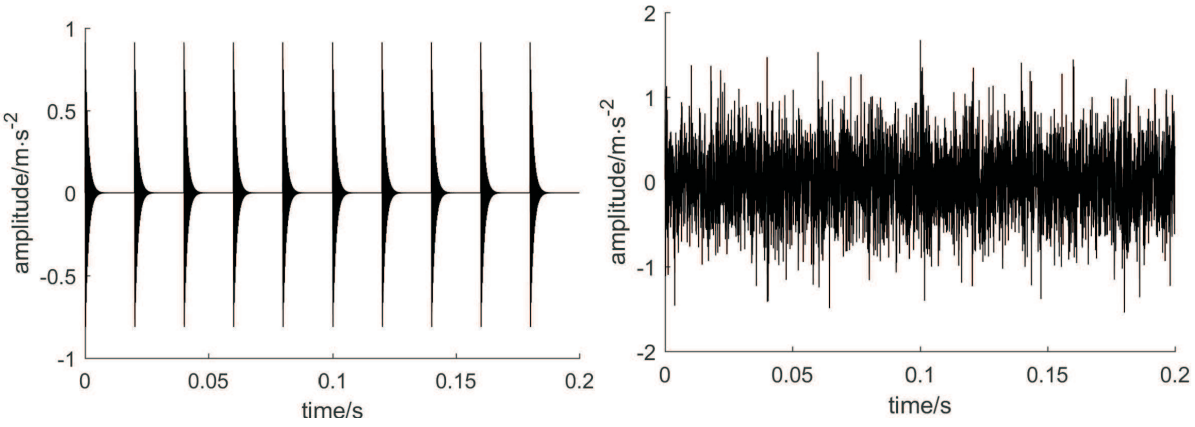

Figure 6: (a) The fault impulse; (b) The simulation signal of additive noise.

The fault signal $x_2(t)$ has been overwhelmed by heavy background noise so the denoised method is proposed. To determine the approximate period of the impulse

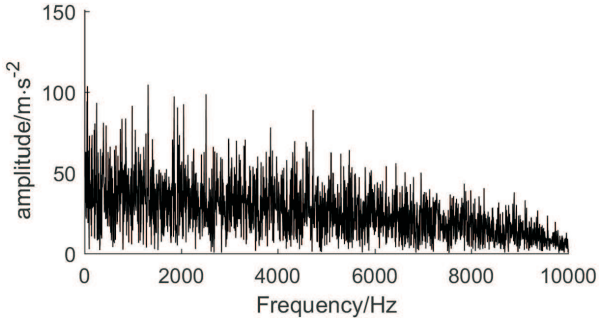

Figure 7: The envelope spectrum of the simulation signal.

signal, the Mkurt is performed. The result is shown in Figure 8(a). The peaks occur at the locations of periods 80, 100, 133, 200, 400 and 800, respectively corresponding to 1/5, 1/4, 1/3, 1/2 and integer multiples of the impulses period. To further extract the impulses, a reasonable period interval [390-410] is set according to the estimated period. The MOMEDA denoised method is performed on the simulation signal, and then the IEWT method is performed to decompose the denoised signal into meaningful IMFs. Figure 8(b) is the result of the adaptive spectrum segmentation. It can be seen from the figure that the Fourier spectrum is segmented into fourteen parts in which each part corresponds to a single component.

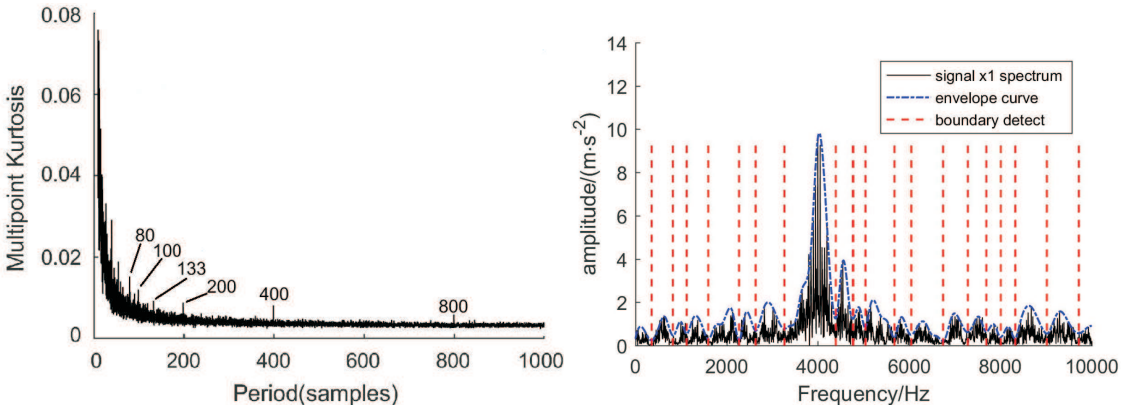

(a) (b)

Figure 8: (a) The result of the Mkurt; (b) The spectrum segmentation based on MOMEDA and IEWT.

Figure 9(a) shows the decomposition result of the IEWT method, due to space limitations, this paper lists only the first six components of the maximum kurtosis value, the imf1-to-imf6 kurtosis value are given in Table 1. It can be seen from the table that the kurtosis value of the imf4 components is the largest. Selecting IMF4 components as a sensitive component is to further perform Hilbert envelope spectrum analysis, the results is shown in Figure 9(b), in which the amplitude of the fault frequency f_i and its

frequency multiplication (labeled as $2f_i$, $3f_i$, $4f_i$ and $5f_i$) are all very large, fault features are well extracted.

Table 1: The kurtosis value.

IMF	Imf1	Imf2	Imf3	Imf4	Imf5	Imf6
K	3.11	3.45	3.33	5.78	3.38	3.30

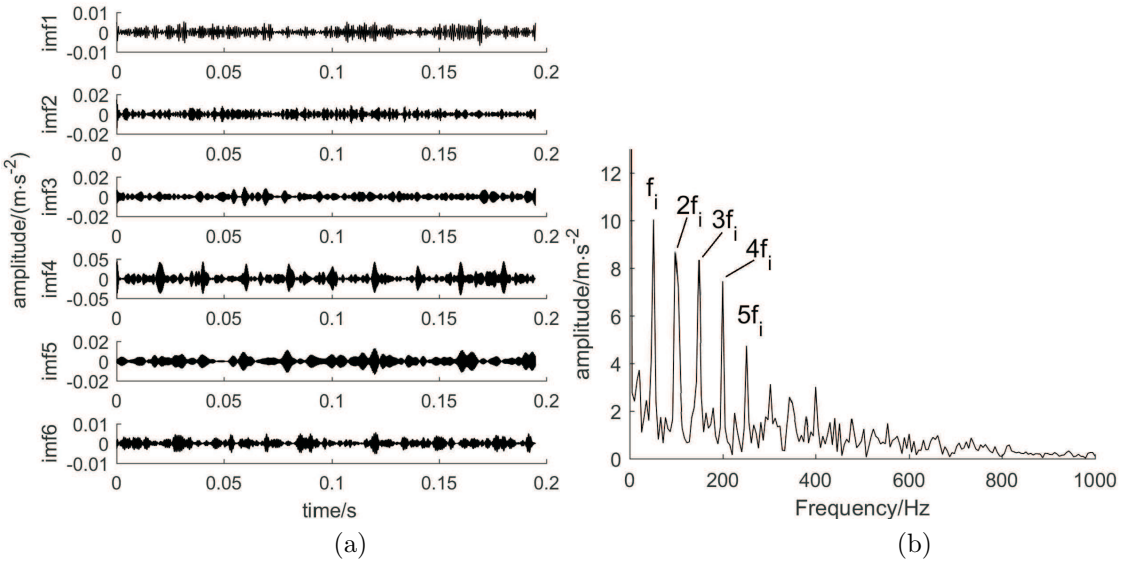

Figure 9: (a) The IEWT decomposition result; (b) The result of the envelope spectrum.

For the comparison, The EMD method is used to decompose the denoised signal, as shown in Figure 10. Due to limited space, only the first six components are enumerated. The first three IMFs components contain most of the fault information, and the fault features of the remaining components are not obvious and exist the false components beyond understanding which is not conducive to later analysis.

The simulation results show that when the impulses reflecting fault features is overwhelmed in the background of heavy noise and other strong vibration components, the peaks of the Fourier spectrum are not obvious, which is unfavorable to accurately segment the spectrum. However, by combining the MOMEDA and IEWT method, the simulation signal is adaptively decomposed into meaningful components, the fault features frequency can be accurately extracted from the envelope spectrum which realizes the effective diagnosis of the bearing.

5 Experimental Analysis

We use the rolling bearing data for experimental verification. The basic layout of the Bearing Test Rig is shown in Figure 12, including a 2 hp Electric motor, a torque

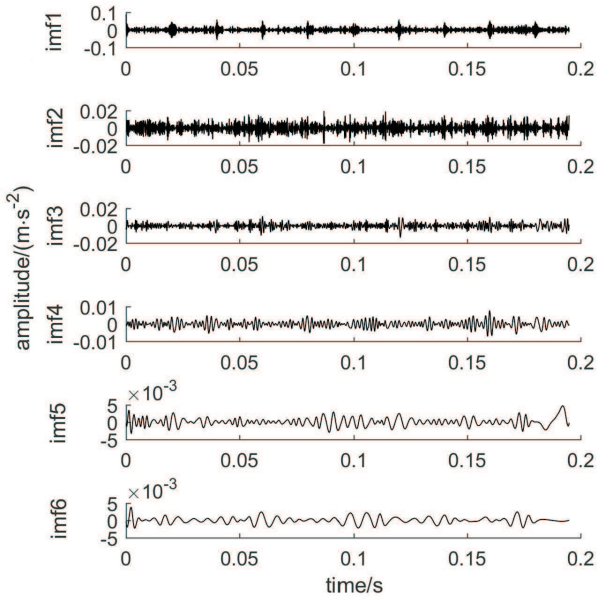

Figure 10: The decomposition result based on MOMEDA and EMD.

transducer and encoder, a dynamometer, as well as electronic control system (not shown in Figure 11). The tested bearing supports the shaft of the motor. The drive end bearing type is SKF6205. An acceleration sensor is placed above the bearing seat on the Electric motor drive end to collect the vibration acceleration signal of the fault bearing. In this paper, the wear data of the inner race of the drive end bearing is analyzed. The rotation speed is 1797 r/min, the damage diameter is 0.007 inch, the sampling frequency is 12 kHz, the inner race fault frequency is 162 Hz, the period is 74, the rotation frequency is 29Hz and the sampling points is 4800.

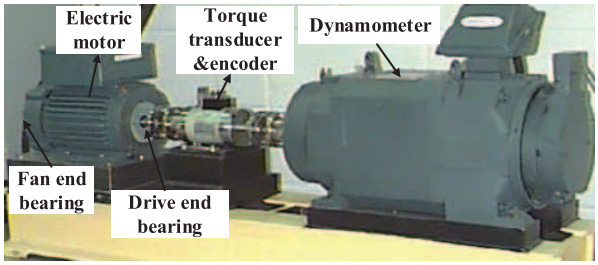

Figure 11: The bearing test rig.

The collected vibration signal of the inner race is shown in Figure 12. We can see that there is only a few impulse components and no regularity. The inner race fault signal performs the Fourier transform, the obtained frequency domain is shown in Figure 13(a) and Figure 13(b), in which we can find that the energy of the signal is basically distributed in the wide frequency range. Since the fault signal has a lot of background

noise, it can only see a few frequency components of outstanding value. Hence, the classic Fourier transform and envelope spectrum analysis cannot effectively extract the fault feature of the signal.

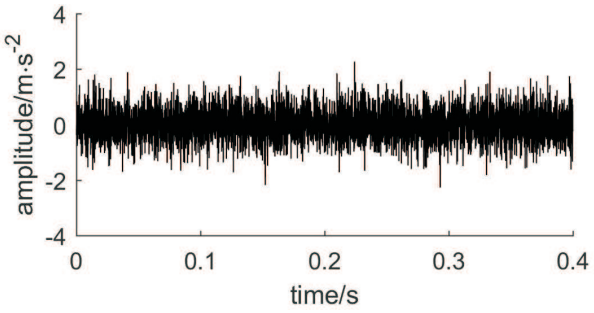

Figure 12: The vibration signal of the bearing inner race.

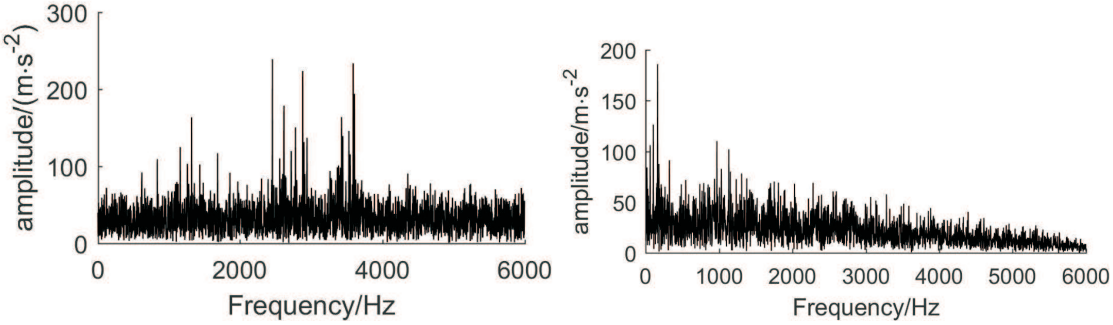

(a) (b)

Figure 13: (a) The frequency domain results of the signal; (b) The envelope spectrum of the signal.

Using the MOMEDA denoised method performs signal processing which effectively extracts extensive impulse components. Firstly, the Mkurt analysis is performed and the result is as shown in Figure 14(a), it can be seen from the figure that the fault period is about 74 and appearing the half and the integer multiplication of the fault period. Then the fault interval further shrinks and is restricted to a range of [70-78]. Finally, the fault signal is denoised by the MOMEDA method, a large amount of noise is removed, as shown in Figure 14(b).

The denoised vibration signal is decomposed into meaningful mode components by the IEWT method, as shown in Figure 15. It can be seen from Figure 15 that the fault impulses periodically appears. Due to the limited space, only the first six IMFs components with the largest kurtosis value are listed in this paper. The kurtosis values are shown in Table 2 and we can see that the imf4 kurtosis value is maximum. The Hilbert envelope spectrum is employed to analyze IMF4 component, the result is shown in Figure 16, in which it can be clearly seen that the bearing rotational frequency f_r,

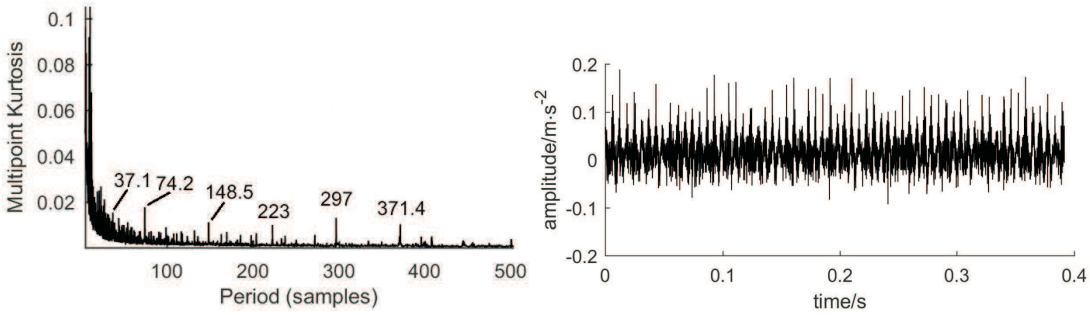

(a) (b)

Figure 14: (a) The result of the Mkurt; (b) The result of the denoised signal.

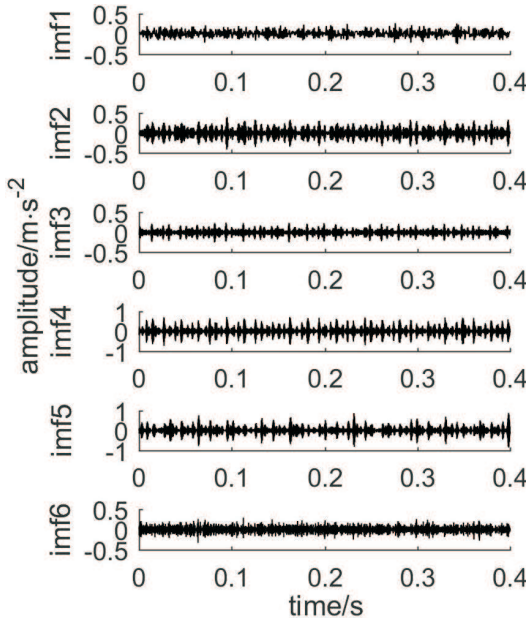

Figure 15: The decomposition results based on MOMEDA and IEWT.

the fault feature frequency and its frequency multiplication are obvious at the spectrum, which can clearly determine that the bearing inner race occurs the fault and coincide with the actual situation.

Table 2: The kurtosis value.

IMF	Imf1	Imf2	Imf3	Imf4	Imf5	Imf6
K	2.65	3.46	4.64	5.70	5.38	5.03

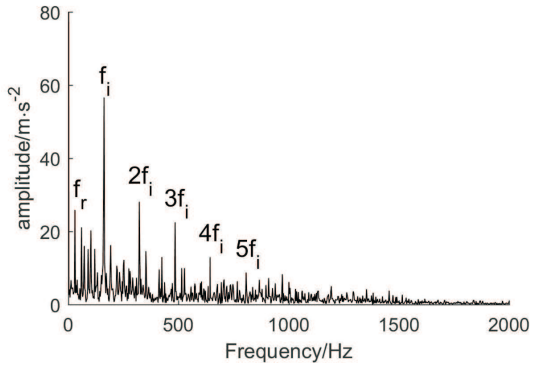

Figure 16: The result of the envelope spectrum.

6. Conclusions

(1) Aiming at the problem of early weak fault of non-stationary vibration signal in complicated and heavy noises, a rolling bearing fault diagnosis technology based on MOMEDA and IEWT is proposed. The simulation and test results show that this method is feasible and effective.

(2) The MOMEDA method can identify the periodic impulses, using the Mkurt method is to estimate the approximate period of the fault, and then control the locations of deconvolution by setting a reasonable period interval of the fault to accurately achieve denoised signal.

(3) The IEWT method is used to solve the problem of the spectrum segmentation, and the method of selecting sensitive components is given, which improves the accuracy of the Hilbert envelope spectrum analysis.

(4) Due to the time relationship, this paper only uses the MOMEDA method to achieve accurate denoise and the IEWT method to achieve modal decomposition. However, it cannot implement self-adaptive features extraction and intelligent diagnosis of faulty conditions. It needs to be future studied in the future, such as applying deep learning theory.

Acknowledgements

This work was financially supported by The National Natural Science Foundation of China and the Civil Aviation Administration of China joint funded projects (U1733108), Tianjin Science and Technology Support Program Key Project (16YFZCSY00860), Natural Science Foundation of Tianjin (17JCQNJC04300), Natural Science Foundation of Tianjin (16JCYBJC18400), Open Funding of the State Key Laboratory of Mechanical Transmissions (SKLMTKFKT-201616).

References

[1] Cabrelli, and Carlos, A. (2012). Minimum entropy deconvolution and simplicity: a noniterative algorithm, GEOPHYSICS, Vol.50, 394-413.

[2] Gilles, J. (2013). *Empirical wavelet transform*, IEEE Transactions on Signal Processing, Vol.61, 3999-4010.

[3] Hu, Z. B., Xu, M. X., Jiang, G. D. and Zhang, D. S. (2014). *Analysis of non-stationary signal of a sudden unbalanced spindle based on wavelet noise reduction and short-time fourier transformation*, Journal of Vibration & Shock, Vol.33, 20-23+36.

[4] Li, Y., Xu, M., Liang, X. and Huang, W. (2017). *Application of bandwidth emd and adaptive multiscale morphology analysis for incipient fault diagnosis of rolling bearings*, IEEE Transactions on Industrial Electronics, Vol.64, 6506-6517.

[5] Ma, L., Kang, J., Meng, Y. and Lv, L. (2013). *Research on feature extraction of rolling bearing incipient fault based on morlet wavelet transform*, Chinese Journal of Scientific Instrument, Vol.34, 920-926.

[6] Ma, Z., Liu, X., Li, Y. and Zhang, J. (2017). *Rolling bearing fault feature extraction based on variational mode decomposition-wavelet packet transform and energy operator demodulation*, Journal of Graphics, Vol.38, 174-179.

[7] Mcdonald, G. L. and Zhao, Q. (2017). *Multipoint optimal minimum entropy deconvolution and convolution fix: application to vibration fault detection*, Mechanical Systems & Signal Processing, Vol.82, 461-477.

[8] Ren, X., Wang, C., Zhang, Y. and Wang, J. (2017). *Incipient fault diagnosis of rolling bearings based on dual-tree complex wavelet packet transform adaptive teager energy spectrum*, Journal of Vibration & Shock, Vol.37, 735-742.

[9] Shi, P., Ding, X., Li, G. and Han, D. (2013). *An improved method of emd and its applications in rotating machinery fault diagnosis*, Journal of Vibration & Shock, Vol.32, 185-190.

[10] Shi, Y. (2014). Machinery Fault Diagnosis Technology and Application, 1st Edition, Beijing: National Defend Industry Press.

[11] Shi, P., Yang, W., Sheng, M. and Wang, M. (2017). *An enhanced empirical wavelet transform for features extraction from wind turbine condition monitoring signals*, Energies, Vol.10, 972.

[12] Wang, Z., Han, Z., Liu, Q. and Ning, S. (2014). *Weak fault diagnosis for rolling element bearing based on med-eemd*, Transactions of the Chinese Society of Agricultural Engineering, Vol.30, 70-78.

[13] Wang, Y., Chen, W., Sun, C. and Huang, H. (2017). *Early weak fault diagnosis of gearboxes based on energy aggregation and EWT*, China Mechanical Engineering, Vol.28, 1484-1490.

[14] Wang, Z., Wang, J., Zhao, Z., Wu, W., Zhang, J. and Kou, Y. (2017). *Composite fault feature extraction of gear box based on MKurt-MOMEDA*, Journal of Vibration Measurement & Diagnosis, Vol.37, 830-834.

[15] Wang, Z., Zhang, Q., Xiong, J., Xiao, M., Sun, G. and He, J. (2017). *Fault diagnosis of a rolling bearing using wavelet packet denoising and random forests*, IEEE Sensors Journal, Vol.17, 5581-5588.

[16] Zhang, Z., Shi, X., Shi, Q. and Tang, B. (2012). *Fault feature extraction of rolling element bearing based on improved emd and spectral kurtosis*, Journal of Vibration & Shock, Vol.31, 80-83.

[17] Zhao, H. and Li, L. (2017). *Incipient bearing fault diagnosis based on MCKD-EMD for wind turbine*, Electric Power Automation Equipment, Vol.37, 29-36.

[18] Zheng, J., Pan, H., Yang, S. and Cheng, J. (2017). *Adaptive parameterless empirical wavelet transform based time-frequency analysis method and its application to rotor rubbing fault diagnosis*, Signal Processing, Vol.130, 305-314.

[19] Zhu, W. and Feng, Z. (2016). *Fault diagnosis of planetary gearbox based on improved empirical wavelet transform*, Chinese Journal of Scientific Instrument, Vol.37, 193-2201.

Department of Mechanical Engineering, Tianjin Polytechnic University, China.

E-mail: shangzhiwu@126.com

Major area(s): Fault diagnosis, product development.

Department of Mechanical Engineering, Tianjin Polytechnic University, China.

E-mail: gengruigr@163.com

Major area(s): Fault diagnosis, product development.

Department of Mechanical Engineering, Tianjin Polytechnic University, China.

E-mail: 835484705@qq.com

Major area(s): Fault diagnosis, product development.

Department of Mechanical Engineering, Tianjin Polytechnic University, China.
E-mail: 758247040@qq.com
Major area(s): Fault diagnosis, product development.

Department of Mechanical Engineering, Tianjin Polytechnic University, China.
E-mail: 1060243807@qq.com
Major area(s): Fault diagnosis, product development.

Department of Mechanical Engineering, Tianjin Polytechnic University, China.
E-mail: Yunjintian_tju@163.com
Major area(s): Dynamics and control of multibody systems, machine vision.

(Received September 2018; accepted November 2018)